GEOPHYSICS, VOL. 74, NO. 1 (JANUARY-FEBRUARY 2009); P. E45–E56, 21 FIGS., 2 TABLES.
10.1190/1.3002769

Acoustic waves in sand-screened deepwater completions: Comparison of experiments and modeling

Andrey Bakulin[1], Dmitry Alexandrov[2], Alexander Sidorov[2], and Boris Kashtan[2]

ABSTRACT

Real-time completion monitoring with acoustic waves has been proposed recently as a method to monitor permeability changes along completions. Typical deepwater completions contain additional layers of sand screen, gravel sand, and perforated casing, which make them quite different from a fluid-filled open borehole. Monitoring changes in flow properties across the completion is crucial because impairment of permeability in any of these layers could cause reduced well productivity. In contrast to an open-hole model, a sand-screened completion supports two tube waves related to an inner fluid column and a gravel suspension in the annulus. To study effects of screen and sand permeability on tube-wave signatures, we construct simple numerical models of various completion scenarios using poroelastic descriptions of screen and sand. Models generally predict that a fast tube wave does not attenuate at either low or high permeability, but experiences resonant attenuation at intermediate frequencies. In contrast, a slow tube wave attenuates completely above a certain permeability value. Models provide a qualitative and sometimes a semiquantitative description for signatures of the fast tube wave. However, they are unable to explain why the slow tube wave is observed in experiments with high permeabilities of sand and screen. We speculate that a better model of complex sand screens is required to match experimental data.

INTRODUCTION

Real-time completion monitoring (RTCM) using tube-wave signatures was proposed by Bakulin et al. (2008a, 2008b, 2008c, 2008d) as a method to detect impairment (permeability reduction) changes along deepwater completions. Estimation of formation permeability from tube or Stoneley waves is used routinely in open-hole logging (Chang et al., 1988; Tang et al., 1991; Tang and Cheng, 2004; Endo, 2006). An open borehole, with a single fluid column and a single interface between the poroelastic formation and the wellbore fluid, supports a single tube wave. Inside the fluid column, the tube wave consists mainly of a piston-like motion. When the fluid is compressed, it attempts to expand radially and pushes against the formation or casing. When the borehole wall is permeable, the tube wave can exchange fluid with the formation, and this leads to slowdown its velocity and an increase in attenuation. Winkler et al. (1989) showed that Biot theory (Biot, 1956) can provide a satisfactory explanation to experimental observations of tube-wave velocity and attenuation and thus can be used for quantitative inversion of permeability from acoustic data.

In sand-screened completions (Figure 1), there are multiple layers of permeable materials such as sand screen, gravel sand, perforated casing, and formation. Impairment or reduction in permeability of each of these layers or boundaries can reduce flow rates greatly and lead to serious underperformance of deepwater wells (Wong et al., 2003). Permanent pressure and temperature data cannot characterize the impairment in detail unambiguously, thus limiting progress in resolving these challenges.

Bakulin et al. (2008d) suggest that acoustic data have the potential to characterize the impairment in greater detail and in real time. In order to realize this potential, acoustic signatures of realistic deepwater completions need to be understood properly. Bakulin et al. (2008a, 2008d) examine in detail a sand-screened completion without a gravel pack. They used an experimental setup consisting of two concentric pipes (sand screen and casing) with two fluid columns and introduced an analytical model describing the case of an impermeable screen. They showed that, because of the presence of two fluid columns and two pipes, there are two tube waves at low frequencies: fast and slow. Because fast and slow tube waves respond differently to permeability changes in various completion layers, they extended this model further, using numerical poroelastic simulations to treat the case of a permeable slotted sand screen. In addition, they showed that such a model predicts anomalous attenuation

Manuscript received by the Editor 2 April 2008; revised manuscript received 25 May 2008; published online 12 December 2008.
[1]Formerly at Shell International Exploration & Production Inc.; presently at WesternGeco, Houston, Texas, U.S.A. E-mail: abakulin@slb.com.
[2]St. Petersburg State University, Department of Geophysics, Saint-Petersburg, Russian Federation. E-mail: dalexandrov@earth.phys.spbu.ru; asidorov@earth.phys.spbu.ru; kashtan@earth.phys.spbu.ru.

of the fast tube wave in the medium frequency range correctly. The frequency band of anomalous attenuation is controlled by screen permeability. However, poroelastic modeling failed to predict signatures of the slow tube wave supported by the screen. Although modeling predicted almost complete attenuation of the slow tube wave, experiments revealed a detectable slow arrival with relatively large amplitudes. Although we expect that the description of sand screens needs to be improved, we still consider such a model a good starting point to analyze the effect of gravel sand on acoustic signatures.

Bakulin et al. (2008a, 2008d) hypothesize that gravel sand should have a small but nonzero shear velocity. In this case, only a single tube wave exists, with properties that are affected by all completion layers. However, actual experiments with sand-screened completions (Bakulin et al., 2008b, 2008c) revealed two clear tube-wave arrivals, thus suggesting that perhaps gravel sand has a negligible shear velocity and acts largely as a fluid suspension. This was an important experimental finding, because completion with two fluid columns (fluid inside the screen and gravel-sand suspension in the annulus) supports two tube waves similar to an earlier model and experiments without a gravel pack (Bakulin et al., 2008a, 2008d).

In this study, we attempt a more systematic analysis of tube-wave signatures, based on experimental data in gravel-packed completions with realistic wire-wrapped sand screens. We attempt to generalize our simple analytical model to describe these signatures by taking into account the permeable nature of gravel packs and sand screens. Although we observe that both data and models predict tube-wave signatures to be highly sensitive to permeabilities of both screens and gravel sand, it remains clear that a better description for sand screens is required to obtain quantitative agreement.

EXPERIMENTAL SETUP

Figure 2 shows a sketch and photo of the full-scale laboratory setup of a completed horizontal well. The outside consists of a 30-ft aluminum outer pipe (casing) with perforations, and the inside has a sand screen and gravel pack. Other details of the experimental setup are pictured in Figure 3. Acoustic measurements are performed with 24 fiber-optic sensors (Figure 3a) wrapped around the outer pipe (casing), as described by Bakulin et al. (2008d). The sensor spacing is 38 cm. On the outside of the pipe, the tube or "breathing" waves have mainly radial motion. Minute expansion or contraction of the pipe volume is picked up reliably by 10 m of wrapped sensing fiber (Figure 3a). Wire-wrapped sand screen is placed inside the casing (Figure 3b) and consists of an aluminum base pipe with perforations and a plastic wire wrap with 0.2 mm gaps (Figure 3c). To model plugged sand screens, we used a similar but unperforated aluminum base pipe (Figure 3b). The gravel-packing process fills the annulus between the sand screen and the casing (and perforation tunnels in real wells) with high-permeability gravel sand. The sand screen and gravel pack prevent migration of reservoir sand into the wellbore, and they maintain the structure of the reservoir around the wellbore. Figure 3d shows a picture of a gravel-packed model where a small channel at the top remains free of sand to ensure that proper cleanout can be achieved. Acoustic signals are excited with a piezoelectric acoustic source placed inside the screen (Figure 3e).

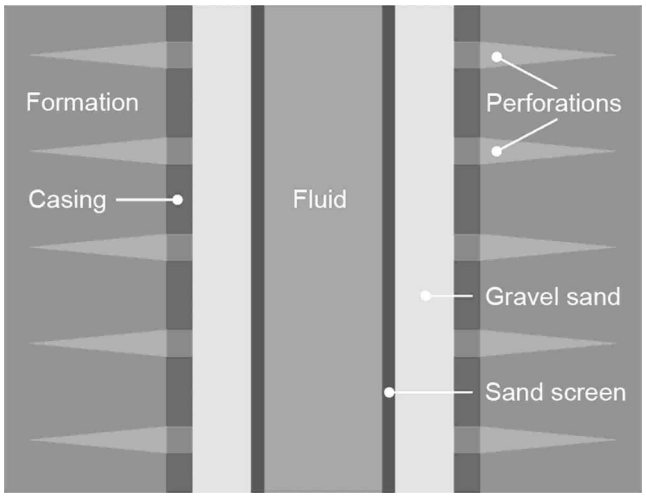

Figure 1. Schematic of a deepwater completion in cased borehole. Note multiple layers of permeable materials (screen, gravel sand, perforated casing) that separate the formation from the wellbore fluid.

SAND-SCREENED COMPLETION WITHOUT GRAVEL PACK

Model

Let us consider an idealized model of a sand-screened completion with a free outer boundary (air) as used in our experiments: fluid, permeable screen, fluid, and casing. Bakulin et al. (2008d) investigate a model for impermeable screen and casing in detail. Following previous studies, we model the sand screen as a layer of poroelastic Biot material with parameters given in Table 1. Average porosity was estimated using simple geometrical computation, whereas other parameters were determined by trial and error to approximate observed mode velocities. At low frequencies, such a four-layered

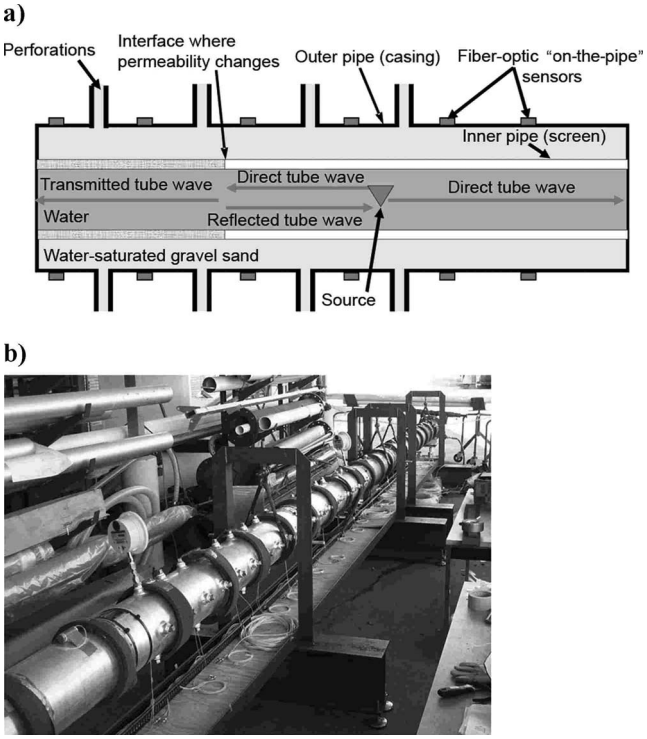

Figure 2. (a) Sketch and (b) photograph of the full-scale laboratory model of a completed horizontal well.

model supports two tube waves and two plate (extensional) waves (Bakulin et al., 2008d). Figure 4a depicts a synthetic seismogram for such a case computed with poroelastic reflectivity modeling that uses full Biot equations (Biot, 1956) including effects of dynamic permeability. Parameters listed in Table 1 follow the notations introduced by Johnson et al. (1987), and computer-code implementation is described by Plyushchenkov and Turchaninov (2000). Fast and slow tube waves propagate without dispersion and attenuation. To compare with experimental results, all synthetic data show the radial component of displacement on the boundary of the outer pipe (casing), because this is the quantity measured by the fiber-optic sensors in Figure 3a. As confirmed by modeling and validated experimentally (Bakulin et al., 2008d), these responses are compatible with those obtained by hydrophones inside the fluid.

To understand the nature of tube-wave modes, it is instructive to analyze the radial distribution of displacements for each mode (Figure 5a). Although Figure 5a shows the distribution of displacements for a poroelastic screen with 10 mD permeability, this picture is almost identical to that for an impermeable screen (0 D[darcy]). Figure 5, which was obtained by reflectivity modeling, describes the behavior of displacements at a frequency of approximately 500 Hz, which is the central frequency of the source signal.

There is a remarkable difference between the two tube-wave modes: the fast tube wave has axial displacements of the same sign inside both fluid columns, whereas the slow wave has displacements of opposite signs. The fast wave is the one that transforms to a regular tube wave when the shear rigidity of the inner pipe goes to zero. Under this transition, the axial displacement in the fast wave becomes equalized in the two fluids and the radial displacement becomes linear (similar to Figure 5c), whereas the propagation velocity remains similar. In contrast, the slow wave displacements and velocity all approach zero while still maintaining the same structure. Therefore we can infer that the fast wave is supported by the outer pipe, whereas the slow one is supported by the inner pipe as originally proposed by Bakulin et al. (2008d).

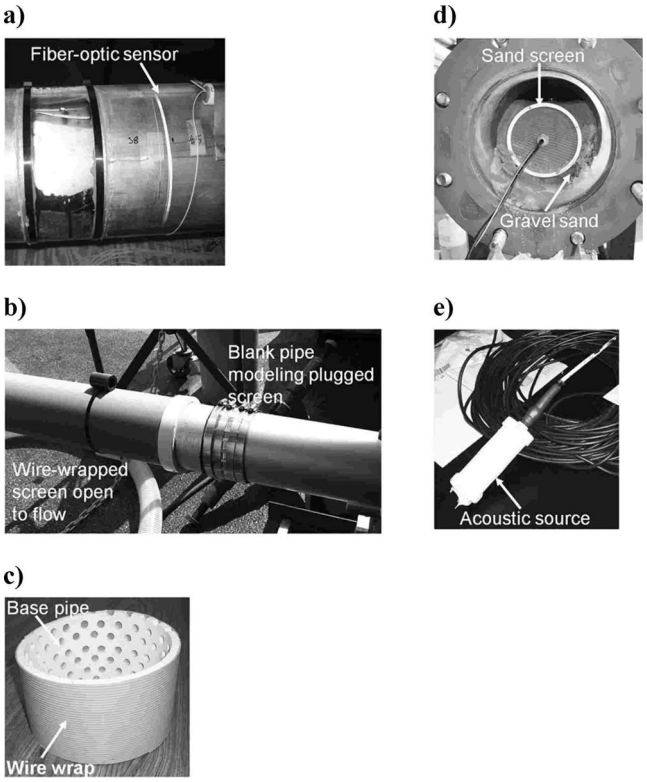

Figure 3. Components of experimental setup: (a) fiber-optic "on-the-pipe" acoustic sensor; glass windows were inserted every 5 ft to observe the gravel-packing process; (b) wire-wrapped sand screen and blank pipe; (c) cross section of the screen showing wire wrap and base pipe (although a plastic base pipe is shown, an aluminum one was used in the experiment); (d) gravel-packed annulus; (e) piezoelectric acoustic source.

Table 1. Material properties used for modeling.

Parameters	Gravel sand	Fluid "sand"	Aluminum screen	Fluid-filling in porous layer	Aluminum
Bulk modulus K (GPa)		6.5		2.25	66.4
Shear modulus μ (GPa)					25.6
Density ρ (kg/m^3)	2052	2052	2480	1000	2700
Grain bulk modulus K_g (GPa)	37		66.4		
Grain shear modulus μ_g (GPa)	44		25.6		
Grain density ρ_g (kg/m^3)	2670		2700		
Dry bulk modulus K_0 (GPa)	1.35		50.9		
Shear modulus μ (GPa)	0.01		19.4		
Porosity	0.37		0.13		
Viscosity (Pa s)				0.001	
Tortuosity	1.5		1.5		
Dynamic permeability parameter M[a]	1		1		
P-wave velocity [saturated, $f = 0$ Hz] (m/s)	1780	1780	5600	1500	6100
S-wave velocity [saturated, $f = 0$ Hz] (m/s)	0		2800		3080

[a]See Johnson et al. (1987), Plyushchenkov and Turchaninov (2000).

When screen permeability increases, both waves start to attenuate (Figure 4b-e), but their dependence on permeability is quite different. To obtain a simple first-order dependence on permeability, we use slowness-frequency and velocity spectra (Figure 6). Velocity is estimated as the speed at which maximum energy is achieved for a particular arrival. For the fast tube wave in Figure 6b, it is 1090 m/s. The energy attribute simply denotes the value of the peak for the wave of interest. Normalization is performed with respect to the base case of the impermeable screen. Thus the energy peak of the fast wave in the impermeable model is taken as unity. These simple attributes can be well applied to synthetic and real data equally, because averaging over multiple receivers and over the entire range of frequencies makes them robust with respect to noise.

Limits of small- and large-screen permeabilities

The estimated static permeability of open-to-flow wire-wrapped screens is expected to be in the range of 250–1000 D, whereas plugging can reduce it all the way to zero. Varying the screen permeability from 0 darcy to 1000 D, we obtain Figure 7. A vanishing permeability makes the poroelastic screen equivalent to an elastic impermeable solid, for which both tube waves should have no attenuation (Bakulin et al., 2008d). Alternatively, the same state can be achieved

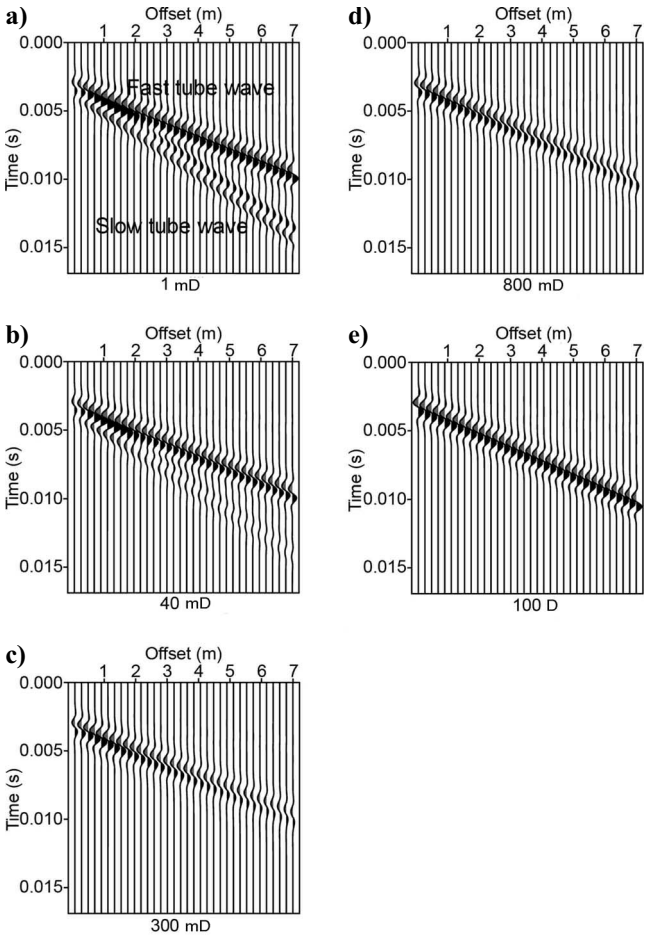

Figure 4. Synthetic seismograms of radial displacement on the outer pipe in a model of sand-screened completion without gravel pack. Here and below, the system was simulated as a four-layered model: water, poroelastic screen, poroelastic sand, and elastic aluminum. Material and geometric parameters of the model are given in Tables 1 and 2, whereas permeability of the screen is varied. Central frequency of the monopole source is 500 Hz. Observe that attenuation of the fast tube wave is vanishing at (a) low and (e) very high permeabilities, whereas it is noticeable at the intermediate permeabilities (b through d). In contrast, the slow tube wave has attenuation that increases monotonously with permeability of the screen and becomes almost invisible for permeabilities higher than 300 mD.

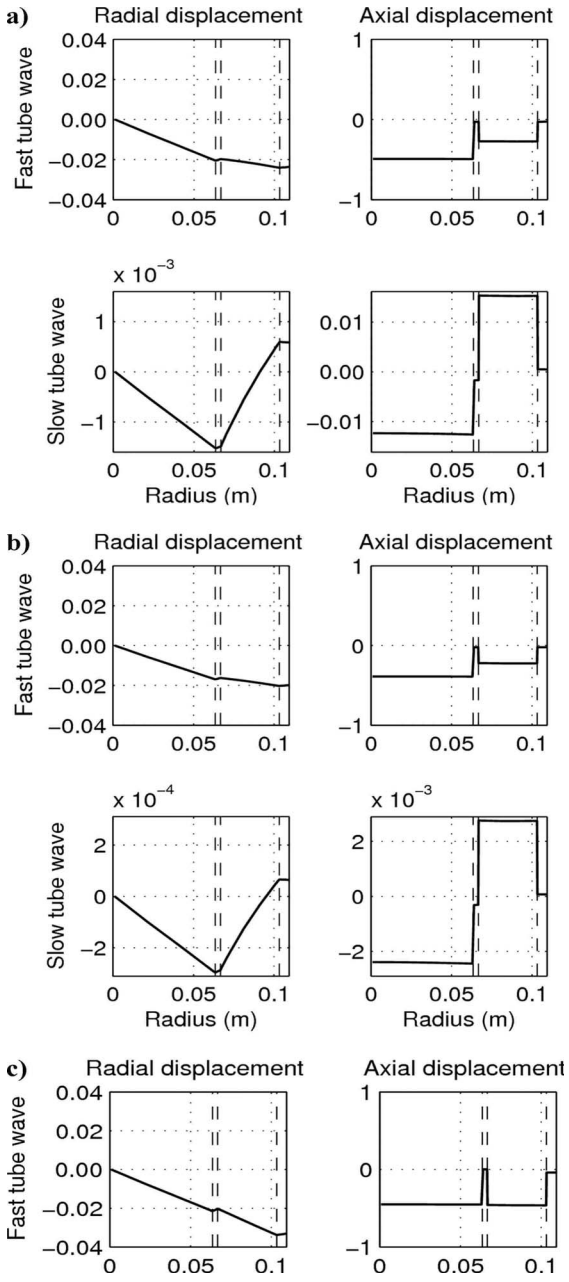

Figure 5. Radial variation of displacements in fast and slow tube-wave modes for models of sand-screened completion without gravel pack with different screen permeabilities: (a) 10 mD, (b) 150 mD, (c) 10 D (slow wave is not shown because of complete dissipation). For poroelastic screen, displacement averaged over solid and fluid phase is shown. It is continuous at the open interface with a fluid. Note that increasing permeability equalizes axial displacement of the fast wave in both fluid columns and leads to a linear profile of radial displacement. In contrast, raising permeability decreases all displacements in the slow wave. Eventually it dissipates this wave completely.

by assigning any permeability to the thin screen and simply setting a closed-pores boundary condition between the screen and the surrounding fluid on either side. At the other extreme, a screen with a very high permeability value is similar to a layer of fluid. It becomes so permeable that it provides almost no resistance to the radial fluid motion across the screen. Figure 8 confirms that replacing the screen with a layer of an equivalent fluid leads to virtually the same acoustic response. Because the fast tube wave is supported by the outer casing, it exhibits no attenuation and dispersion as it should in a liquid-filled cylinder. In contrast, the slow wave, supported by the inner pipe, totally disappears because the screen does not provide any resistance to the radial motion of the fluid to maintain this arrival.

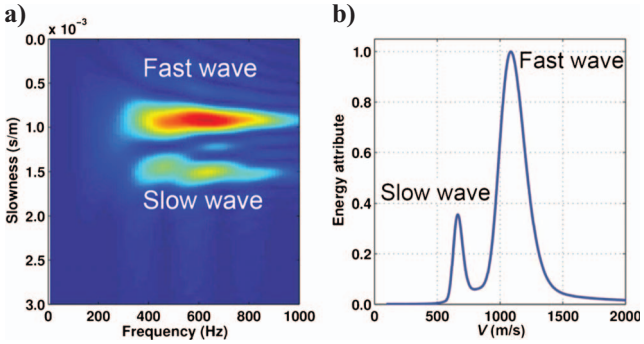

Figure 6. (a) Slowness-frequency display of synthetic data from Figure 4a. (b) Velocity spectra obtained by horizontal stacking of Figure 6a. Two peaks correspond to fast and slow waves respectively. The fast-wave peak provides estimate $V = 1090$ m/s, whereas the slow-wave peak gives $V = 660$ m/s. Energy is normalized so that peak of the fast wave is equal to unity.

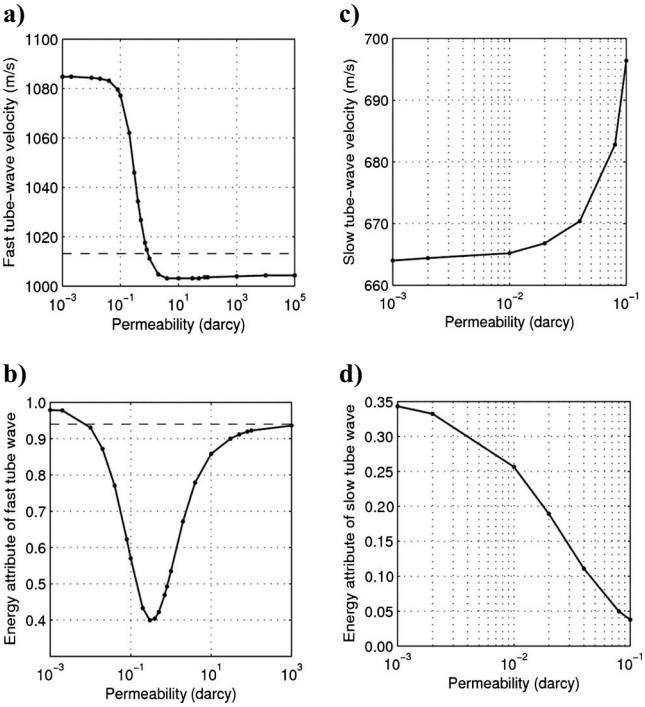

Figure 7. Attributes of the fast (a, b) and slow (c, d) tube waves derived from numerical model of a sand-screened completion without gravel pack as a function of sand-screen permeability. Both attributes are estimated from the peaks of velocity spectra similar to Figure 6b. Energy attributes are normalized with respect to the values in a reference model with an impermeable screen (separate for each wave). Observe that the fast wave does not attenuate at vanishing permeability and very large permeability. In contrast, the slow-wave energy attribute increases with increasing permeability, and this arrival completely attenuates above 0.1 darcies. Dashed line shows corresponding energy and velocity attributes in a model where the screen is replaced by a layer of fluid with the same P-wave velocity and density (Table 1).

Intermediate permeabilities

When the behavior of extreme cases of low and high permeability is understood, it is possible to see what happens at intermediate values of permeability. The slow tube wave experiences a monotonic increase in attenuation with increasing permeability and becomes almost unobservable (as a separate peak) at permeabilities larger than 0.1 D (Figure 7d). This can be explained readily by radial profiles of displacement for this mode (Figure 5). A slow tube wave is analogous to a slow Biot wave in the sense that it has opposite signs of displacement in the two fluid columns. As one can see in Figure 5a, first arrivals in the inner fluid have negative axial displacements; whereas in the outer fluid, axial displacements have opposite signs. When the screen becomes permeable, the fluid on both sides starts to communicate, and this out-of-phase motion leads to strong attenuation. Eventually the attenuation will absorb this wave completely (Figure 5b and c). Note that all values of permeability produce the same character of profile and displacements with opposite signs.

Another observation is that velocity of the slow mode increases with permeability (Figure 7c), which is opposite to tube-wave behavior in simple models of a fluid-filled borehole surrounded by poroelastic formations (Tang and Cheng, 2004). It is also counterintuitive to the usual scenario in which increased attenuation is accompanied by a velocity slowdown. One possible interpretation is that the velocity of the slow mode increases and merges with the fast mode at very high permeabilities, thus collapsing two modes into one.

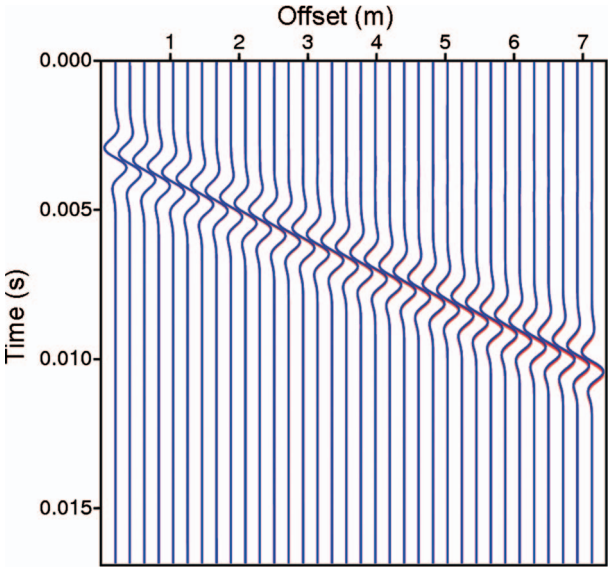

Figure 8. Comparison of seismograms for an open screen of 100 D (red) with the model where the screen is replaced by a fluid layer (blue) with the same longitudinal velocity and bulk density (Table 1). Note the generally good agreement between two sets of waveforms suggesting that the highly permeable screen behaves similarly to the layer of fluid. Note that only the fast tube wave is seen without attenuation and dispersion.

In contrast, the fast wave experiences less drastic changes. Initially the fast tube wave also undergoes increased attenuation with increasing permeability. However this attenuation peaks at about 300 mD and then decreases, returning to the state of virtually no attenuation at large permeability (Figure 7b). To a first degree, the location of the attenuation maximum is controlled by screen permeability and thickness. Radial profiles provide an additional insight on a possible mechanism for this attenuation at intermediate permeabilities. For low permeabilities, axial displacements of the fast wave are of the same sign, but of different magnitudes (Figure 5a). When the screen becomes permeable, the different rates of compression inside the two liquid columns lead to a fluid exchange across the screen. This exchange intensifies particularly near 300 mD, which is manifested by rapid equalization of axial displacements occurring in this region (Figure 9). At high permeabilities, the axial displacement becomes constant (Figure 5c), whereas the radial displacement resembles the linear profile typical for a conventional weakly dispersive unattenuated tube wave in a fluid-filled cylinder (Figure 8).

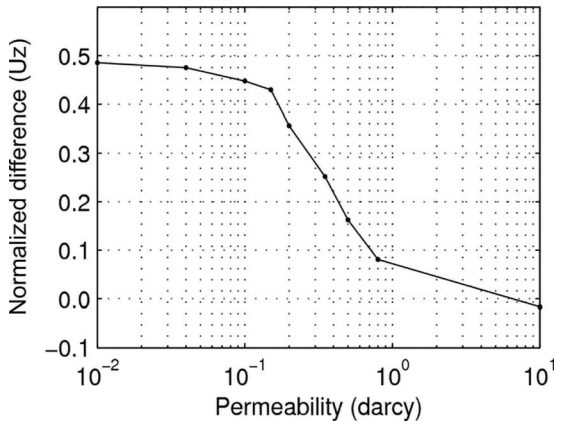

Figure 9. Difference between axial displacements in inner and outer fluids as a function of screen permeability in a model of sand-screened completion without gravel pack. The difference is normalized by the maximum axial displacement for each value of permeability. Observe rapid equalization of displacement near critical permeability of 300 mD where energy has minimum (Figure 7b). At higher permeability the difference is almost zero, indicating that piston-like motion of two fluid columns occurs in complete synchrony.

Next let us compare predictions of these simple models with the experimental data.

Comparison with experiment: Impermeable screen (blank pipe)

Figure 10a shows experimental seismograms for a blank pipe that simulates an impermeable screen. Two arrivals are recognizable on the background of crisscrossing reflections from various pipe joints. The slowness-frequency display (Figure 11a) suggests that the slow wave has a lower frequency, whereas the fast wave has higher-frequency content with reduced energy at the medium frequency range (500–700 Hz). Such behavior is similar to that observed in slotted sand screens (Bakulin et al., 2008a, 2008b). Velocity spectra (Figure 11a) confirm the presence of two arrivals with velocities ~1000 m/s and 700 m/s. In addition, we note the agreement of experimental velocity spectra (Figure 11a) with similar results from synthetic modeling (Figure 6).

Comparison with experiment: Open-to-flow wire-wrapped sand screen

In the presence of an open-to-flow wire-wrapped screen, the acoustic response changes substantially (Figure 10b). Let us review which numerical predictions are in agreement and disagreement with the experiment. First, Figure 10b has an amplitude level similar to that of Figure 10a. This agrees with predictions from Figure 7b, suggesting that open-to-flow sand screens (~250–1000 D) should lead to small energy loss in fast tube waves. Second, Figure 7a predicts reduction in velocity of the fast wave, which is seen in the experiment also (Figures 10b and 11c), albeit to a larger extent.

There are also disagreements between modeling and experiment, particularly concerning the behavior of the slow tube wave. Modeling suggests that this arrival is fully attenuated at permeabilities larger than 0.1 D (Figure 7d). However, experimental data (Figure 10b) clearly shows a low-frequency slow arrival. The limited number of traces does not allow us to resolve fast and slow waves on a slowness-frequency display or velocity spectra (Figure 11c). Instead,

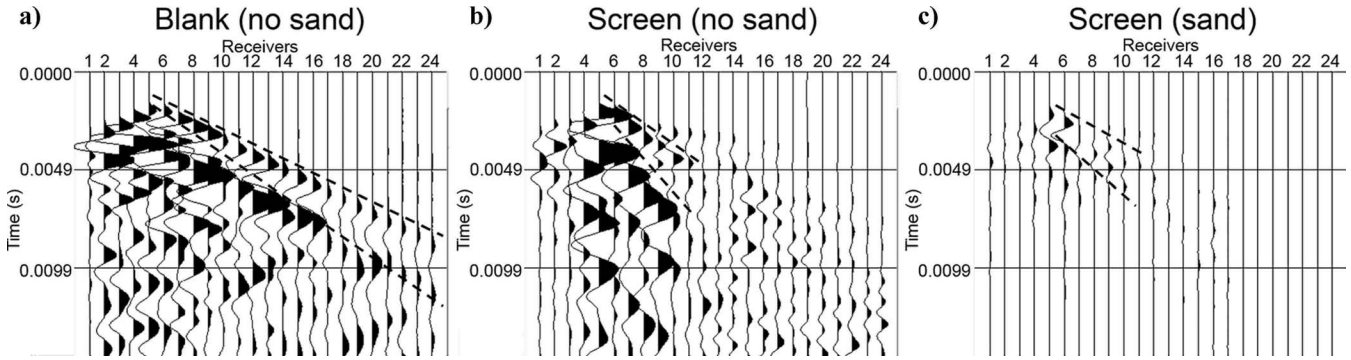

Figure 10. Experimental seismograms in different completion models from the same source near receiver 5 shown with identical magnification: (a) entire completion has impermeable screen (blank pipe) with no gravel sand. Velocities of fast and slow tube waves are ~1000 m/s and 700 m/s respectively. (b) There is still no gravel pack in this model, whereas the blank pipe between receivers 1 and 12 is replaced by a section of open-to-flow wire-wrapped screen. In the open-screen section, both fast and slow tube-wave velocities are slowed down to ~700–800 m/s and 400–600 m/s respectively. (c) Same model as (b), with open-screen section between receivers 1 and 12, but with gravel pack. Velocities are similar to the case (b). Note that two arrivals of fast and slow tube wave are visible on both displays. Observe the increase in attenuation with introduction of the screen section in (b) and the even larger increase when adding sand in (c).

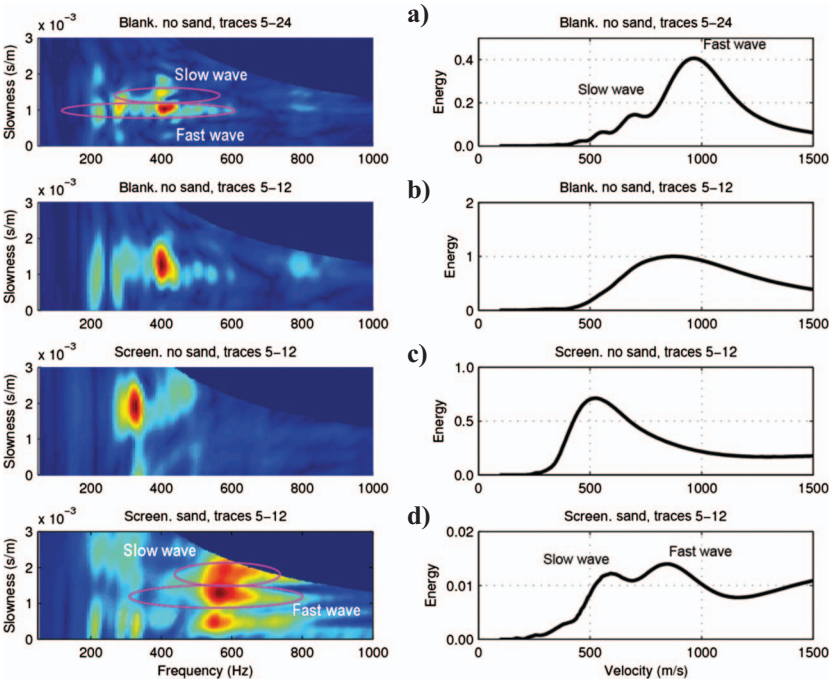

Figure 11. Pairs of slowness-frequency and velocity-spectra displays for various experimental completion models. Plots (a) and (b) are for completion with impermeable screen (blank pipe) without gravel pack and only differ by the number of traces used. Note that the use of more traces (a) resolves peaks for fast and slow tube waves and velocity spectra looks similar to the modeled result from Figure 6. Plot (c) depicts completion with permeable screen without sand, whereas plot (d) shows gravel-packed completion with open screen. Because (b–d) use the same number of traces and normalization, their energy peaks can be compared directly. For example, we observe the shift to low frequency and slowdown in velocities when the plugged screen (b) is replaced by the open screen (c). Even greater attenuation is seen when sand is added in (d).

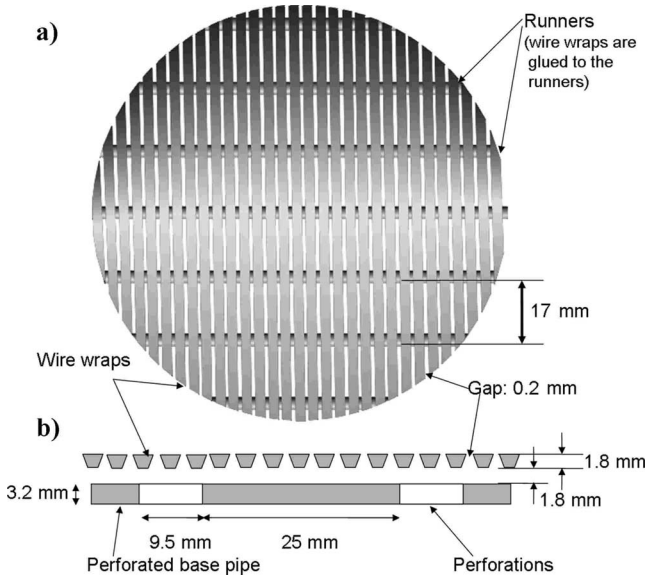

Figure 12. Actual design of a wire-wrapped screen used in the experiment: (a) map view and (b) cross-section. The inner layer is perforated aluminum pipe (base pipe), followed by an annulus filled partially with axial PVC runners, and an outer layer of wire wrap with gaps determined by size particles of formation and gravel sand.

Figure 11c shows a broad peak that lumps two arrivals together. Second, velocities of both fast and slow arrivals are substantially lower in the experiment.

This overall picture is quite similar to the initial set of experiments (Bakulin et al. 2008a, 2008d) that were performed with different types of sand screen, represented by slotted water screens. Previous results suggest that a poroelastic description might be appropriate for the fast tube wave. However, the slow tube wave was seen in the experiment but not predicted by modeling.

We conclude that both sets of experimental data suggest that such simplistic poroelastic modeling of sand screens is clearly deficient, especially as far as the slow tube wave is concerned. In addition, we stress that more realistic wire-wrapped screens used in current experiments have the complex structure shown on Figure 12. The structure consists of three main layers: an inner layer of perforated aluminum base pipe, a free annulus with axial runners, and an outer layer of wire wrap. There are various other designs of sand screens. For simplicity in the numerical model, we used a poroelastic aluminum-like layer only, with a thickness equal to the thickest layer of the base pipe, and ignored the two outer layers (Table 2). However, the estimated (static) permeability included the effects of all three layers. A model of parallel slits or fractures (van Golf-Racht, 1982) in a homogeneous impermeable background was used to estimate the permeability of the wire-wrap layer. Likewise, a model of a bundle of capillary tubes (Bear, 1988) was used for the base pipe. Then the average permeability of the entire screen was computed for radial serial flow through a three-layer system (Ahmed, 2001). More complicated two- and three-layer models of the screen were also simulated, but conceptually, these results were close to the simple one-layer model of the screen and are not included here.

One can see clearly that the most likely screen cannot be modeled by effective media because dimensions of wire wrap, gaps, and perforations are of the same order or larger than thicknesses of the screen layers. Therefore the size of the "sample" (screen thickness) is smaller than a representative volume (see chapter 2.1, Zinszner and Pellerin, 2007) although all of the microstructural features are much less than a typical wavelength (~1–2 m). In addition, we find it challenging to define average dynamic (acoustic) permeability of

Table 2. Geometry and material composition of the setup.

	Model of experiment setup	
Cylindrical layers	Material	Outer radius, (m)
Layer 1	Water	0.0635
Layer 2	Aluminum sand screen	0.0667
Layer 3	Water/gravel sand	0.1032
Layer 4	Aluminum casing	0.1095

the screen and to relate it to a meaningful low-frequency or static permeability (from flow and pressure). It is also likely that we would need to account for substantial anisotropy in transport and mechanical properties. Nevertheless we anticipate that some kind of effective description for the screen must exist, because clearly we see only several well-formed arrivals. We hope that future research will be able to resolve these challenges.

SAND-SCREENED COMPLETION WITH GRAVEL PACK

In the same manner, we analyze the behavior of completions with gravel pack (Figure 3d). Sand screen and gravel pack prevent the migration of reservoir sand into the wellbore, and maintain the structure of the reservoir around the wellbore. Another objective of these completions is to diffuse the velocity of the flow entering the wellbore (especially through perforations) and protect the sand screen from erosion. Thus it is important to see whether the gravel pack was placed properly, and whether it remains in place. If the gravel sand is washed away, it might create so-called "hot spots" of high-velocity streams that can erode the screen quickly and lead to sand production (Wong et al., 2003). Replacing failed screens is an expensive workover that can cost $30–40 M USD. In another scenario, formation sand can mix with gravel sand or replace it. Permeability of the gravel sand is ~100–500 D, and formation sand can be as low as ~1 D. If this impairment happens, then the flow bypasses areas of low permeability and redirects it to unimpaired zones instead. A flow velocity that is too high can fluidize the gravel sand and create unsafely high flow velocities (Wong et al., 2003). Bakulin et al. (2008b, 2008c) present experimental data suggesting that active and passive surveillance with RTCM can detect many of these scenarios potentially and thus serve as an important input to optimize completions practices and drawdown strategies for expensive deepwater wells.

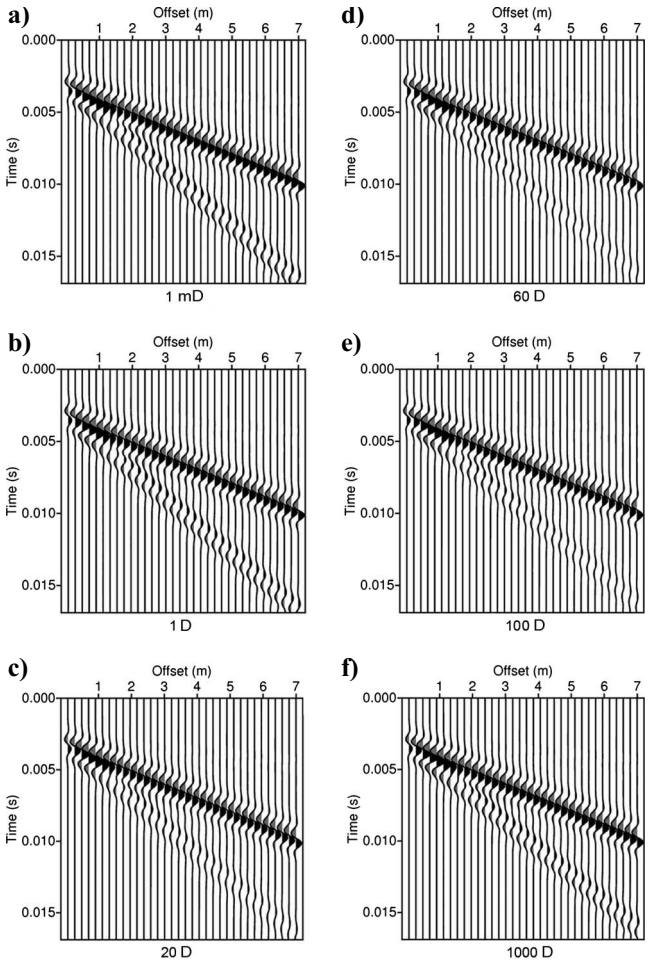

Figure 13. Synthetic seismograms of radial displacement on the outer pipe in a model of gravel-packed completion with an impermeable sand screen. Central frequency of the monopole source is 500 Hz. Parameters of the model are given in Tables 1 and 2. Observe that attenuation of the fast tube wave is vanishing at (a) low sand permeability. In (b) through (d), it is noticeable at intermediate permeabilities, and it is vanishing again at (e) very high sand permeability. In contrast, the slow tube wave attenuation increases monotonously with permeability of the screen and becomes almost invisible for permeabilities higher than 300 mD.

To analyze the effect of gravel sand, we modify the previously used four-layer model by replacing the annulus fluid with a poroelastic layer simulating gravel sand. Defining the shear-wave velocity in the water-saturated gravel sand is crucial. Bakulin et al. (2008d) speculate, based on the literature and some guided-wave measurements, that the velocity might be a small but nonzero value, on the order of 30–80 m/s. Wave-propagation modeling with such a velocity revealed a single tube wave and a single plate (extensional) wave, as though the signal were propagating in a composite multilayered pipe. Nonzero shear rigidity of the gravel sand makes it look as if the layered completion (screen, gravel, casing) acts as an effective (anisotropic) elastic pipe. Although tube-wave velocity remains close to the fast tube-wave velocity in a model with two fluids, the plate-wave velocity slows down substantially and the slow tube wave disappears. In contrast to these predictions, experiments by Bakulin et al. (2008b, 2008c) reveal that both tube waves are seen. Also, the plate-wave velocity remains close to its value without sand. All of these experimental findings suggest that the shear velocity of gravel sand is negligible. We measured the porosity of the gravel sand, and an approximate value for permeability was taken from Sparlin (1974). Properties of pure quartz were used for grains, whereas other parameters were obtained easily by assuming a reasonable P-wave velocity for a water-saturated sand (Table 1). In this study, we applied a simple model simulating gravel sand as a poroelastic material with zero shear rigidity and study the effect of gravel and screen permeabilities on tube-wave signatures.

Model of gravel-packed completion with impermeable screen

Figure 13 shows synthetic seismograms for a model with gravel-packed completion when the sand screen is completely impermeable, and Figure 14 shows energy and velocity attributes as a function of gravel-sand permeability. Despite the fact that both screen and casing are impermeable, we observe a surprisingly large effect of gravel-sand permeability, in particular on the slow tube wave. We observe that in the limit of small and large permeabilities, the energy of fast and slow tube waves does not attenuate. This can be given the following physical interpretation. When the permeability is very low, fluid and solid phases of the sand should move in synchrony and simulate an effective fluid because of the frame's zero-shear rigidity. Both energy and velocity attributes match quite well with their counterparts for a model with the sand replaced by an equivalent fluid. For very large values of permeability, the fluid phase can move free-

ly through the gravel layer and be close to the behavior of a lossless fluid, albeit with a slightly different velocity. At intermediate values of permeability, relative fluid motion in the pores leads to substantial attenuation of both arrivals — particularly that of the slow tube wave (Figure 14c). Figure 15 confirms that viscous forces keep fluid and skeleton displacements the same until ~ 10 D. A further increase in permeability brings us to the high-frequency regime where the central frequency of the source (500 Hz) is close to or higher than the Biot critical frequency of the sand. In this regime, the fluid has the freedom to move much more intensely, and this initial unlocking is accompanied by an attenuation peak (Figure 15). Once the fluid is fully unlocked, the attenuation disappears as it starts to move freely in the same manner as in a fluid layer. Figure 16 verifies that displacement profiles are almost identical when highly permeable gravel sand is replaced by an equivalent fluid with the same density and P-wave velocity.

Comparison with experiment

In the experiments, we did not vary the permeability of the gravel sand. However, we conducted acoustic measurements during the entire gravel-packing process. One such experiment consisted of gravel packing the blank pipe (Bakulin et al., 2008b). Before packing, we filled the annulus with water of infinite permeability. At the end of gravel packing, the annulus was full of gravel sand with permeability ~200–300 D. Making the simple assumption that the combination of gravel and water layers spans the range of permeabilities from infinity to 200 darcies during the entire gravel packing process, we can compare the conducted experiment to the theoretical model with varying permeability of sand in the annulus (Figure 14).

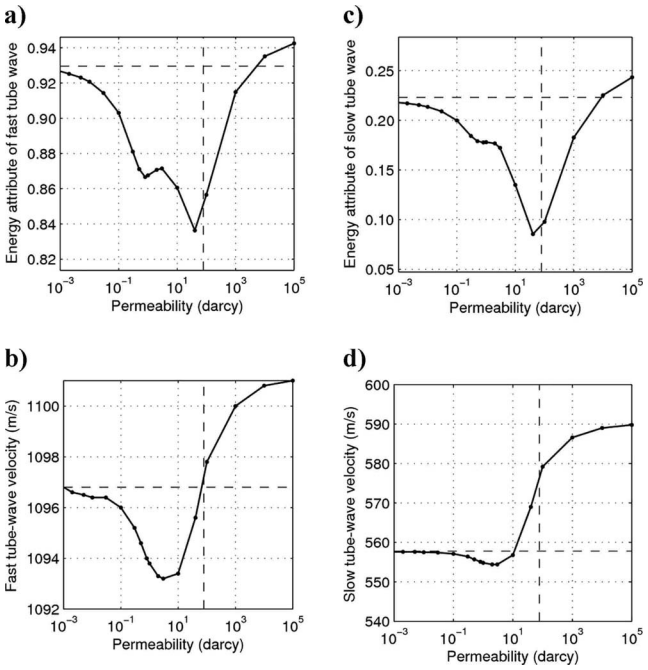

Figure 14. Attributes of (a) and (b) fast tube waves and (c) and (d) slow tube waves derived from numerical model of gravel-packed sand-screened completion with an impermeable screen (0 D) as a function of gravel-sand permeability. Attributes picked from velocity spectra of a corresponding arrival. Vertical dashed line shows permeability (80 D) at which the critical Biot frequency of gravel sand becomes equal to the central frequency of the source (500 Hz). Horizontal dashed line denotes corresponding attributes for a model where the poroelastic sand layer is replaced by an equivalent fluid with the same longitudinal velocity and bulk density. Note the large effects of gravel-sand permeability on tube-wave signatures despite the fact that both screen and casing are impermeable.

Figure 17 presents experimental data at four times during various stages of the gravel-packing process. The dotted box above the plots shows the extent of the model where gravel sand has reached maximum height. Ahead of this large front, we have a sand layer of smaller height. One can clearly observe a dim amplitude anomaly associated with the section in which the annulus is packed only partially with sand. The anomaly moves across the model ahead of the front with maximum packing. The movie shows the acoustic response during the entire gravel-packing process and confirms that a dim spot anomaly moves continuously throughout the model during gravel packing. This anomaly disappears once maximum height is reached across the entire setup.

We observe a good match between theoretical predictions and experimental data. Experiments reveal very similar attenuation and velocities in the extreme cases of water-filled and gravel-sand-filled

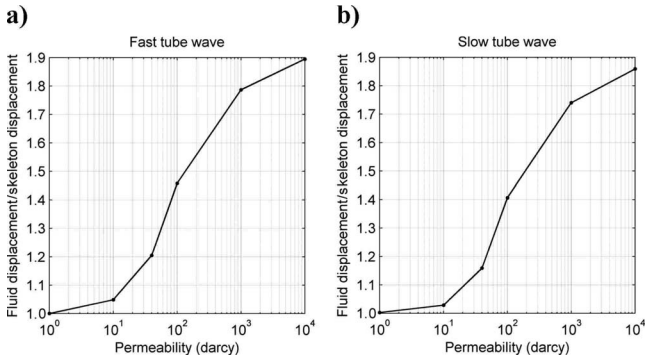

Figure 15. Ratio of average fluid-to-skeleton axial displacement inside the gravel-sand layer for (a) fast and (b) slow tube waves as a function of sand permeability. Model used is the same as in Figure 14 — gravel-packed sand-screened completion with an impermeable screen (0 D). Note that fluid motion gradually unlocks from skeleton especially upon reaching a critical Biot permeability (~ 80 D) for the central frequency of the source (500 Hz).

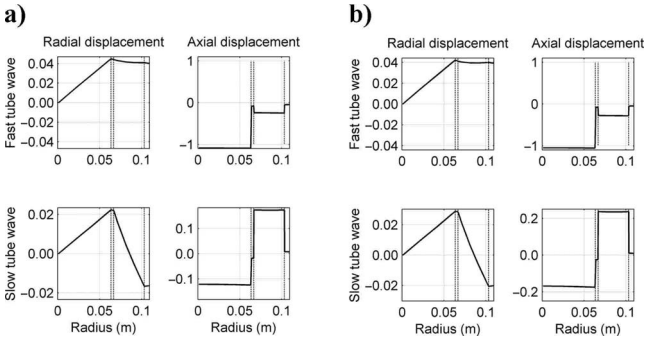

Figure 16. Comparison of radial variation of displacements in fast and slow tube-wave modes for models with impermeable sand screen: (a) annulus is filled by gravel sand with permeability of 10,000 D, (b) annulus is filled with an equivalent fluid. Note excellent agreement between the two sets of displacements confirming that at high permeability, gravel sand behaves like a layer of fluid. Note that inside the gravel-sand layer, average displacements over fluid and solid phase are shown.

annuli (Figure 18a). This is consistent with predictions from modeling for large and small permeabilities (Figure 14a and c). Somewhere between these limiting values of water (infinite) and sand permeability (200 D), we hit "critical permeability" with maximum attenuation and observe low amplitudes (dim anomaly) of both arrivals (Figure 17). Likewise, modeling predicts an energy trough for both the fast and slow waves (Figure 14a and c). Experimental data suggest that "critical permeability" is somewhere above 200 D, although the model predicts it at ~ 40 D (Figure 14a and c). Despite a factor of five or more discrepancy, these estimates are in reasonable agreement after noting that the numerical model is axisymmetric, whereas the actual model is stratified and three dimensional. Also, the presence of a sand-free channel (Figure 3d) might contribute further to the discrepancy. This agreement confirms that the poroelastic description of gravel as a Biot material is adequate. In addition, we note much better agreement in the case of blank pipe (impermeable screen), suggesting that much larger discrepancies with permeable screens are likely because of crude screen modeling.

Figure 18b also allows us to observe the effect on velocities of replacing water in the annulus with sand: we see no change in the fast-wave velocity but observe a measurable decrease in the slow arrival with sand. This behavior can be explained by elastic modeling also. Because P-wave velocities of sand and water are close, the main parameter controlling this change is the bulk density of the annulus fluid. Figure 19 shows that, after replacing water by sand, both tube-wave velocities decrease. However, the fast wave drops by 3% (35 m/s), whereas the slow wave decreases by ~ 22% (140 m/s). Although there is no quantitative match, both data and model agree in predicting little to no change in the fast wave and a noticeable decrease in the slow-wave velocity. On the other hand, similar behavior can be explained by the influence of permeability alone. Figure 14b and d suggest that, at the limit of high permeability (water), both velocities are higher than at lower permeability (gravel sand), with a larger magnitude difference in the slow tube wave.

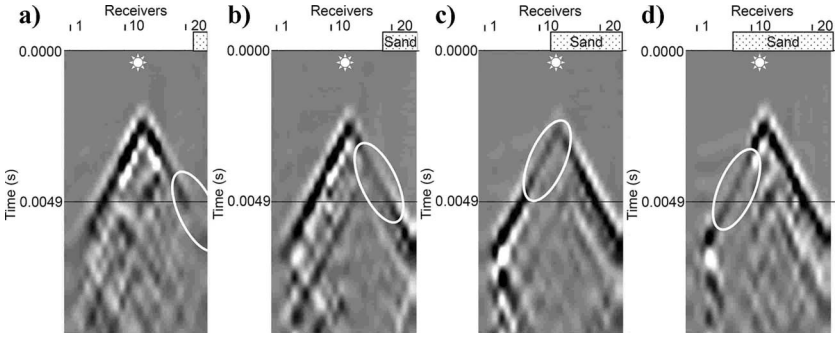

Figure 17. Acoustic responses in a model of a completion with blank pipe at various consecutive stages of gravel packing process. Sand is injected from the right side. The dotted box shows the part of the model with maximum gravel packing. The part of the model to the left of the box contains some limited amount of gravel. Observe the dim spot anomaly associated with the partially packed area of the model. Figure enhanced online.

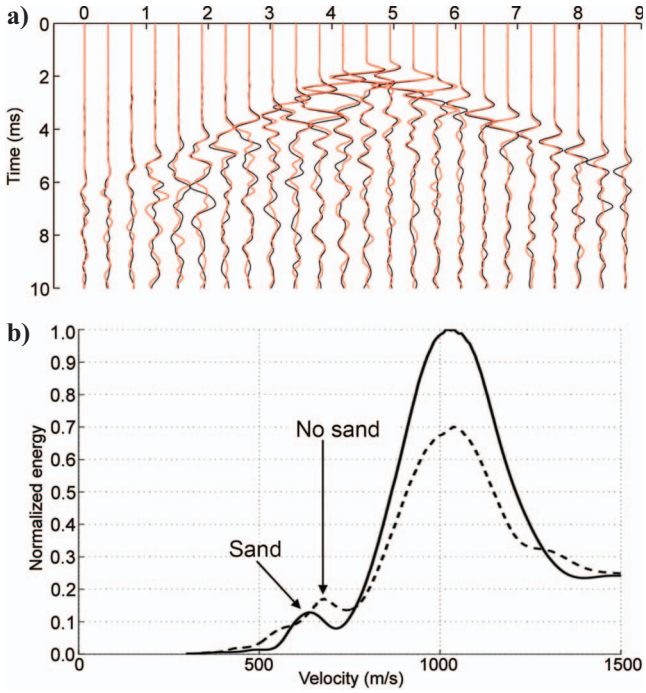

Figure 18. (a) Comparison of experimental seismograms for a completion with impermeable screen (blank pipe) in the presence (black) and absence (red) of gravel pack. (b) Corresponding velocity spectra for these two cases. Observe very similar attenuation in both cases. Note that fast tube-wave velocity is almost unchanged whereas slow tube-wave velocity is decreased slightly by the presence of sand according to the theoretical prediction from Figure 19.

Model of gravel-packed completion with permeable screen

Figure 20 shows predicted velocities and energy attributes for a gravel-packed completion with an open sand screen (100 D). We observe no attenuation at very low and high permeabilities, but for different reasons. Low permeability restricts the movement of the fluid

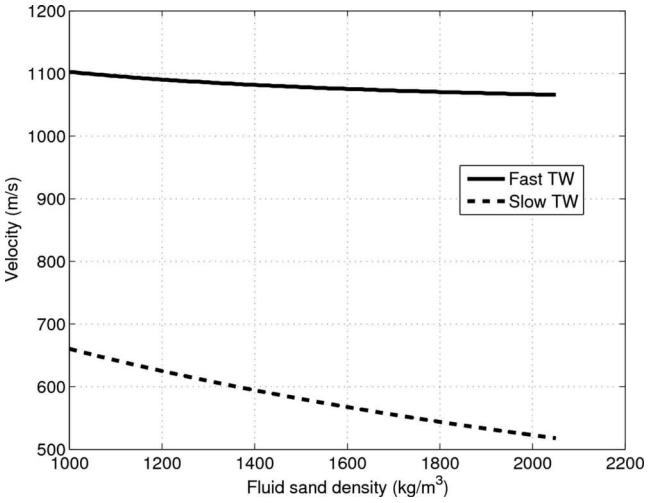

Figure 19. Dependence of tube-wave velocities on the density of the annulus fluid in the model of two concentric pipes and two fluids (Table 2). Left bound of this plot corresponds to the case when both fluids are represented by water. Then density of the annulus fluid is increased all the way to match the density of water-saturated sand (2050 kg/m^3) while all other parameters are kept constant. Screen is modeled by a solid impermeable material with velocities and density from Table 1.

with respect to the solid inside the sand layer (Figure 21). Therefore, although both fluid and gravel sand have zero-shear rigidity, the boundary between open-screen and low-permeability gravel sand behaves as a closed-pore boundary, and no fluid exchange takes place between the inner liquid column and the fluid phase inside the gravel sand.

When permeability increases, such a fluid exchange becomes increasingly possible, introducing large attenuation of the fast wave and absorbing the slow wave completely. Indeed, Figure 21 demonstrates that below 10 D, motions of fluid and solid phases are coupled completely. Above 10 D, the central frequency of the signal (500 Hz) exceeds the critical Biot frequency of the sand, and a rapid increase in relative motion (Figure 21) creates an attenuation peak of the fast wave (Figure 20b). A further increase in permeability allows the fluid to move as freely as it moves inside a skeleton with infinite permeability, and attenuation of the fast wave disappears. Therefore, in the limit of a very large permeability, both the sand and the screen form a very permeable layer that behaves similarly to a layer of fluid. Thus we observe no attenuation of the fast wave, although the slow wave is absent, similar to the case when the screen is replaced by a fluid layer (Figure 8).

Comparison of completions with and without gravel pack

For an impermeable screen, we have seen a small difference in acoustic responses of completions with and without gravel pack (Figure 18a). In contrast, such a difference is substantial in the case of an open-to-flow screen, as shown on Figure 10b and c. Two arrivals with similar velocities are visible on both responses. The most notable impact of the gravel sand is strong attenuation of both modes and, in particular, of the slow mode. Figure 11c and d confirms that low frequencies (300–400 Hz) dominating the slower arrival without sand (Figure 11c) are noticeably absent on the response with the sand (Figure 11d) that is instead dominated by higher frequencies (500–700 Hz). Although Figure 11d shows the presence of two peaks with velocities ~800 m/s and 600 m/s, these velocities are not very reliable because of the limited number of traces. For the same reason, we cannot observe separate peaks on the response without sand (Figure 11c).

Comparing such behavior with the model from Figure 20, we observe the following similarities: Without the gravel pack, the annulus is filled with water (infinite permeability). This can be likened to a gravel pack with very high permeability, which should have little attenuation (Figure 20b). Indeed, Figure 20b for a sand-filled and Figure 7b for a water-filled annulus at high screen-and-gravel permeabilities show very similar behavior. The experimental plot (Figure 10b) confirms this expectation and verifies that relatively little attenuation is observed with respect to the reference case of a blank pipe (Figure 10a). In contrast, replacing the water with sand reduces the permeability from infinity to ~200 darcies, which can approximated as moving from a high to a medium permeability in Figure 20b. At these intermediate permeabilities, we observe greatly increased attenuation of the fast wave, which is in qualitative agreement with the experiment. Similar to previous observations with screens, the discrepancy in the behavior of the slow tube wave remains. As before, we observe a slow tube-wave arrival in experiments with open screens, whereas the model predicts its complete absorption.

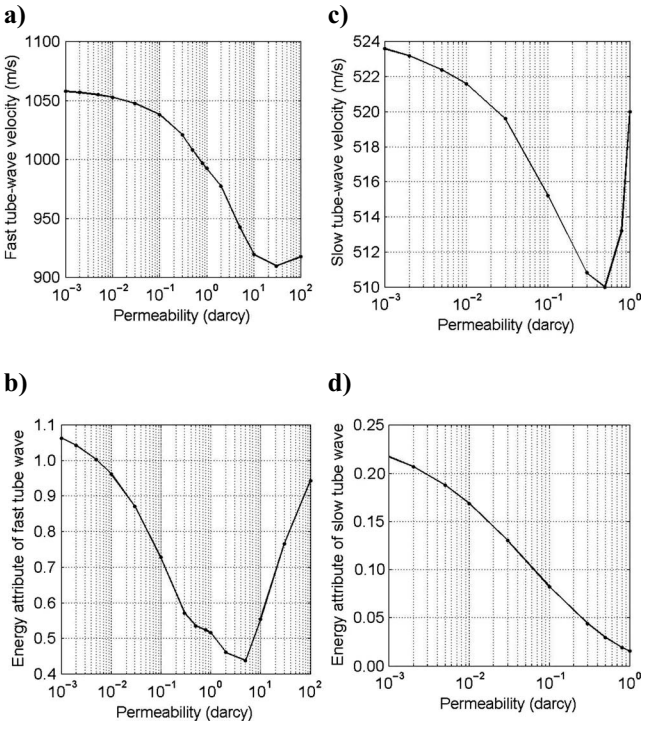

Figure 20. Velocity and attenuation attributes for gravel-packed, sand-screened completion with open screen (100 D) as a function of sand permeability. Other parameters are as in Table 1 and 2. Note that the slow wave attenuates monotonically with permeability increase and becomes unobservable above 1 D, similar to the case of no gravel pack (Figure 7). The fast tube wave experiences strong attenuation peak at ~5 D, but becomes free of losses at the limit of low and high gravel-sand permeabilities.

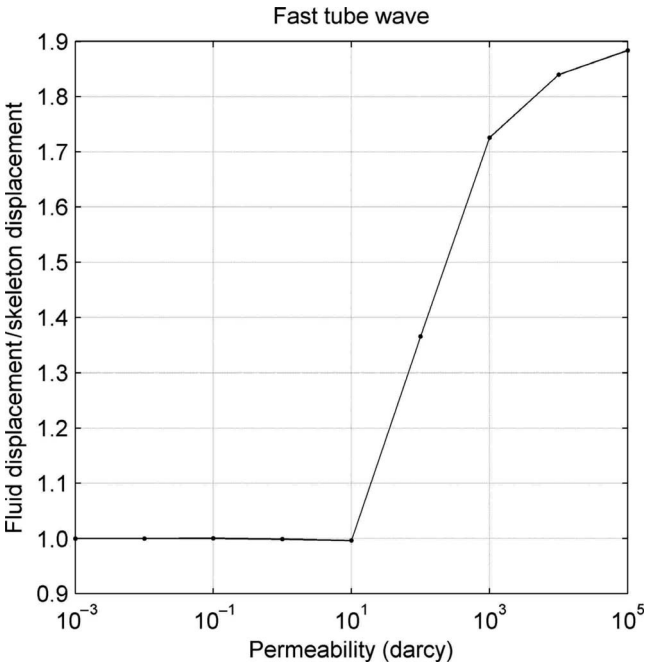

Figure 21. The ratio of average fluid-to-skeleton axial displacement inside the gravel-sand layer for the fast tube wave as a function of sand permeability. The sand screen has permeability of 100 D, other parameters are listed in Tables 1 and 2. Note that fluid motion gradually starts unlocking from solid near permeability ~10 D where the fast wave experiences an attenuation peak from skeleton.

CONCLUSION

We examined borehole wave propagation in sand-screened and gravel-packed deepwater completions, based on full-scale laboratory experiments and poroelastic numerical modeling. Both experiments and models confirm that at low frequencies propagation is dominated by fast and slow tube waves supported by columns of inner fluid and gravel-sand suspension. Velocities and, in particular, the attenuation of the two arrivals is influenced strongly by the permeability of the sand screen and gravel pack. Thus, inversion of tube-wave signatures has the potential to monitor changes in gravel-pack and sand-screen permeabilities. We built several numerical models of various completion scenarios by utilizing a poroelastic description for screens and sands and studied the effect of screen and gravel-sand permeability on tube-wave signatures. Modeling predicts that the fast tube wave is characterized by having the same sign displacements inside the two fluid columns and thus is similar to a conventional tube wave in an open hole. In contrast, the slow tube wave is predicted to have opposite signs of displacements inside the two fluid columns. This unusual character leads to a very strong predicted dissipation of the slow tube wave for screen permeabilities larger than 0.1–1 D, irrespective of whether the annulus is filled with water or gravel pack. In contrast, the fast tube wave experiences a pronounced attenuation peak at these intermediate permeabilities but turns into a conventional unattenuated tube wave at higher permeability, because a highly permeable screen behaves like a layer of fluid.

These modeling predictions can explain qualitatively most of the experimental data conducted with fully open and fully plugged sand screens, with and without gravel pack. However, a striking discrepancy remains: the experimental observation of a slow tube wave with open screens that modeling predicts should be attenuated. We think the culprit is in the overly simplistic description of sand screens in our model. Indeed, replacing the blank pipe with a permeable screen is the step in which the largest discrepancies are observed between data and models. Replacing the water with gravel sand in the presence of impermeable or permeable screens produces results that are in better agreement generally. Therefore, we conclude that a better model of sand screens is required to explain the experimental data. In particular, the relation between dynamic (acoustic) permeability and static permeability needs to be understood for meso-scale structures like screens and perforated casing.

Despite challenges in theoretical modeling of the screens, experiments suggest that the large differences in acoustic signatures between various completion scenarios could be used effectively for acoustic surveillance of completions with RTCM. Similar to the evolution of 4D seismic surveys, we should concentrate on building a larger experimental database to help us improve the modeling capabilities we need for more quantitative descriptions of completion changes. This can be achieved by conducting repeated production logging with existing slim acoustic tools inside the sand-screened completions. If field data confirms laboratory tests fully, then a permanent system can be embedded as a part of a smart completion — for instance, using a fiber-optic acoustic system.

ACKNOWLEDGMENTS

We thank our Shell colleagues Jim Kielty, David Stewart, Jack Boyles, Keith Love, and Ken Wilson for their hard work in creating the experimental setup and assisting with the laboratory experiment. We are thankful to Mikko Jaaskelainen (Shell) and the PGS fiber-optic team for assisting with the development and testing of the fiber-optic acoustic system. We thank Tom Daley of LBNL for providing us with a piezoelectric source and advising us on acquisition. We appreciate assistance by Omer Alpak in estimating screen permeabilities and by Fabian Ernst (both Shell), in coding the slowness-frequency analysis. We are particularly grateful to our colleagues Jorge Lopez, George Wong, and Scott Lester (Shell) for their support of this project.

REFERENCES

Ahmed, T., 2001, Reservoir engineering handbook: Butterworth-Heinemann.

Bear, J., 1988, Dynamics of fluids in porous media: Dover Publications Inc.

Bakulin, A., A. Sidorov, B. Kashtan, and M. Jaaskelainen, 2008a, Acoustic surveillance of production impairment with real-time completion monitoring: Formation Symposium and Exhibition of Formation Damage Control, SPE, paper 112301-PP.

———, 2008b, Downhole acoustic surveillance of deepwater wells: The Leading Edge, **27**, 518–531.

———, 2008c, Real-time completion monitoring estimates production impairment with acoustic waves: Offshore Technology Conference, paper OTC 19213.

———, 2008d, Real-time completion monitoring with acoustic waves: Geophysics, **73**, no. 1, E15–E33.

Biot, M. A., 1956, Theory of propagation of elastic waves in a fluid-saturated porous solid: Journal of the Acoustical Society of America, **28**, 168–191.

Chang, S. K., H. L. Liu, and D. L. Johnson, 1988, Low-frequency tube waves in permeable rocks: Geophysics, **53**, 519–527.

Endo, T., 2006, Evaluation of formation permeability from borehole Stoneley waves: Journal of Geography, **115**, 383–399.

Johnson, D. L., J. Koplik, and R. Dashen, 1987, Theory of dynamic permeability and tortuosity in fluid-saturated porous media: Journal of Fluid Mechanics, **176**, 379–402.

Plyushchenkov, B. D., and V. I. Turchaninov, 2000, Acoustic logging modeling by refined Biot's equations: International Journal of Modern Physics C, **11**, no. 2, 365–396.

Sparlin, D., 1974, Sand and gravel — A study of their permeabilities: AIME Symposium on Formation Damage Control, SPE, paper 4772-MS.

Tang, X. M., and A. Cheng, 2004, Quantitative borehole acoustic methods: Elsevier.

Tang, X. M., C. H. Cheng, and M. N. Toksöz, 1991, Dynamic permeability and borehole Stoneley-waves: A simplified Biot-Rosenbaum model: Journal of the Acoustical Society of America, **90**, 1632–1646.

Van Golf-Racht, T. D., 1982, Fundamentals of fractured reservoir engineering: Elsevier Science.

Winkler, K. W., H. S. Liu, and D. L. Johnson, 1989, Permeability and borehole Stoneley waves: Comparison between experiment and theory: Geophysics, **54**, 66–75.

Wong, G. K., P. S. Fair, K. F. Bland, and R. S. Sherwood, 2003, Balancing act: Gulf of Mexico sand control completions, peak rate versus risk of sand control failure: SPE, paper 84497.

Zinszner, B., and F. M. Pellerin, 2007, Geoscientist's guide to petrophysics: Editions Technip.